On the dynamics of the kite carousel

On the dynamics of the kite carousel

K.N. Luttik
Industrial Doctoral Centre for Offshore Renewable Energy, UK

P.S. Anderson
Scottish Association for Marine Science, Oban, UK

L. Johanning
University of Exeter, Exeter, UK

I.M. Viola
School of Engineering, University of Edinburgh, Edinburgh, UK

ABSTRACT: Kite based generators are being developed as the next iteration of renewable energy converters. One such design is based on generating power by using kites to induce movement in a vertical axis ground based generator, referred to as a kite carousel. This paper introduces a minimum-order model of such a kite and indicates the key scales and parameters that affect the performance of this kite-based generator. The model is validated using experimentally gained data. A physical model is used to determine the aerodynamic coefficients of a high performance kite. The resulting numerical model shows a potential power delivery of 360 W, with substantial room for improving yield.

1 INTRODUCTION

Developments in renewable energy show the importance of pushing the boundaries to find new ways of extracting energy in various locations. In the past decade strides have been made towards developing kite based generation systems as an economic alternative to conventional wind turbines (Khan & Rehan 2016).

Such systems can be divided into one of two designs. A distinction is made according to the placement of the generator. Generation takes place either at the kite, or at ground level. The first design sees the kite acting as a platform for one or multiple turbines. The kite is flown through the airspace allowing the turbines to generate electricity, which is sent down to the surface through a power cable incorporated in the tether.

An alternative design has the generator located at ground level. The kite movement is transferred through the tether to induce motion in the generator. A commonly investigated method is the pumping kite model, where a kite is used to reel out a tether. This tether reel out causes a ground based generator to rotate and generate power. Once the kite is fully reeled out, the kite is retrieved by adjusting the kite attitude and reeling in the tether. This cycle is designed such that there is a net power gain.

Both these designs have been researched extensively and progressed towards early stage commercial development. Much of this research is summarized by Cherubini *et al*. (2015). A substantial amount of research has focused on accurately modelling kite behavior (Argatov *et al.* 2011, Bosch *et al.* 2014, Fechner *et al.* 2014, van der Vlugt *et al.* 2017, Pastor-Rodríguez, *et al.* 2017, Losantos & Sánchez-Arriaga 2015, Cadalen *et al.* 2017, Geschiere 2014). First as proof of concept and subsequently as a basis for the development of kite control strategies. Models range from low-order point mass models (Dadd, *et al.* 2010) to computationally intensive high-order finite element models (Bosch *et al*. 2014).

Thus far, the bulk of research and development has focused on single kite systems. Although, multi-kite systems have been mentioned and studied as a potential way to further increase power output (Cherubini 2017). However, issues with control and lack of firm, validated kite models, have thus far limited the development of many such concepts to full physical models.

This paper describes a low order dynamic model of a kite, which would generate power through a carousel type setup. This setup involves a vertical axis generator where the generating motion comes from one or more kites flying along a flight path that induces motion in the generator. Such a concept was first mentioned by Williams, *et al.* (2007), and Fagiano (2009); Followed by a concept for a large scale carousel by KiteGen (Ippolito 2009, Canale *et al.* 2009).

While both Williams *et al.* and Fagiano investigate carousel designs with high tether length to generator diameter ratios, the resulting control strategies result in substantially different flightpaths. Williams *et al.* seek an optimum flightpath to match generator rotation, leading to quick crosswind loops. Fagiano on the other hand simulates the carousel as a number of vehicles moving along a rail, with power take off

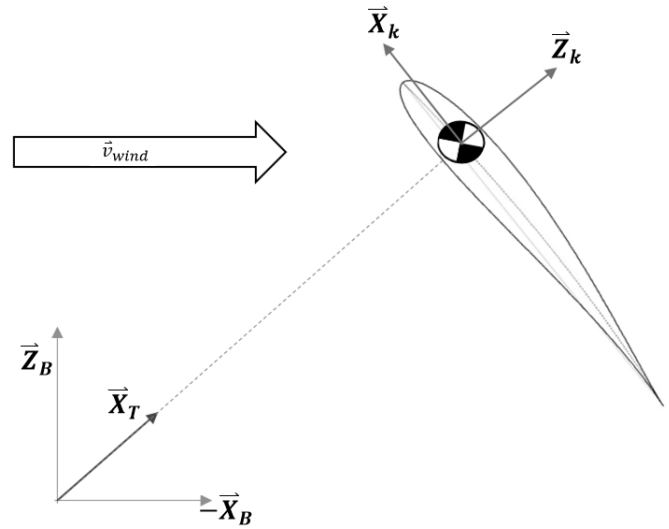

Figure 1: Reference frames used for model.

through the rotation of the wheels while moving downwind. Moving upwind, the vehicles are powered through the rail to pull the kite upwind. As such, two distinct kite behaviours are modelled, with transition phases between them. This results in quick crosswind loops while the kite is moving downwind, and the kite being sent to a stationary zenith position while it is being pulled upwind. Fagiano also includes tether dynamics, where these are excluded from the Williams model. Both models allow for a variable tether length, allowing the models to work as either a pure pumping generator, a pure carousel or a combination of the two. As such, both of these models are computationally intensive.

This paper describes the work that lead to the highly reduced model that was developed to be faster than real time and functions as a first step towards a generic carousel model which can be further developed to demonstrate the feasibility of carousel based generation for tidal applications. To optimize computation time and resources the model was reduced to model only the carousel model. Keeping the tether length at a constant reduced length minimizes the degrees of freedom and consequently keeps the model complexity low. The model is described in section 2. The experimental kite setup used to validate this numerical model is described in section 3. The resulting tuning and validation of the numerical model are shown and discussed in section 4, which are discussed in section 5. Finally, conclusions were drawn in section 6 and, ongoing work and future model progression is highlighted in Section 7.

2 NUMERICAL MODEL

2.1 *Frames of reference*

The axis system used is illustrated in Figure 1, which shows a neutral kite position where $\vec{z}_k$ is in line with the pointing-vector of the tether. This definition of axes is important as with each time step iteration the kite axes position and orientation were updated to represent the kite attitude at the following time step. Kite design allows for manipulation of the power setting, by adjusting the built in angle of attack through manipulation of the kite control lines. In the numerical model this was represented as a rotation around the kite pitch axis $\vec{y}_k$. The base reference was defined by the X-axis ($\vec{x}_k$) pointing directly upwind. The tether vector is indicated by $\vec{x}_T$.

2.2 *Model assumptions*

In order to reduce modelling time, assumptions were made. The assumptions concerning wind profile, kite control, and tether model are described in more detail in the following sections. The model introduced in this paper was designed in such a way that it represents a generic carousel model. For validation purposes the model simulated kite behaviour in air, such that it could be compared to the results of physical kite tests. The kite was modelled as a point mass with a specific aerodynamic profile. Kite control was applied by pitching and rolling the kite to adjust the aerodynamic coefficients and force profiles as described in sections 2.2.2 and 2.2.3.

2.2.1 *Wind profile*

Initially an ideal wind profile was considered, representing a constant uniform flow. To more accurately represent the increase of velocity with height, a log profile was applied as proposed by Stull (2000). The log profile used is shown in equation 1, where the wind velocity ($\vec{v}_{w,k}$) is deduced at kite level (h_k), from the wind measured at ground level ($\vec{v}_{w,g}$ at h_g), and the roughness length ($z_0 = 0.005$) for smooth landscape.

$$\vec{v}_{w,k} = \vec{v}_{w,g} \frac{\ln\left(\frac{h_k}{h_0}\right)}{\ln\left(\frac{h_g}{h_0}\right)} \quad (1)$$

2.2.2 *Power control*

Kite power control was defined as the manipulation of the built in kite angle of attack (α_0). This was done by either adjusting the length of the rear control lines, attached to the trailing edge of the kite; with respect to the main power line, attached at the leading edge of the kite. Lengthening the control lines simultaneously reduces α_0, and consequently the overall angle of attack α, as per equation 2. The reverse is true for shortening the control lines.

The force transmitted through the main power line adjusts due to the effect of the altered angle of attack on the lift and drag coefficients, (C_L and C_D), on overall aerodynamic forces. This effect is further explained in Section 2.3.

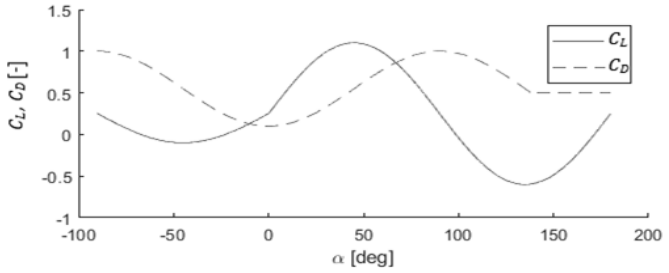

Figure 2: Aerodynamic coefficients used for initial estimation (Fechner 2016, Spera 2008)

The initial aerodynamic coefficients were estimated from literature (Fechner 2016, Spera 2008) and their variation with respect to α is shown in Figure 2 . This graph was eventually tailored to the values deduced from the experimental model. The preliminary graph was used to interpret the initial acceptable working range of α to be $-10° \leq \alpha \leq 20°$. The angle of attack α was computed as

$$\alpha = \alpha_0 + \alpha_w, \quad (2)$$

where

$$\alpha_0 = \sin^{-1}\left(\vec{X}_T \cdot \vec{X}_k\right), \quad (3)$$

$$\alpha_w = \sin^{-1}\left(\frac{\vec{v}_{app} \cdot \vec{X}_T}{|\vec{v}_{app}|}\right), \quad (4)$$

α_w is the angle between the apparent wind vector and the vector perpendicular to the tether from which α_0 is measured. In this case it was important to use the component of the apparent wind speed ($\vec{v}_{app}$) in line with the kite pointing vector ($\vec{X}_k$). The apparent wind speed was computed through $\vec{v}_{app} = \vec{v}_{w,k} - \vec{v}_k$.

2.2.3 *Turning control*

Turning dynamics of a flexible kite have been modelled and approximated extensively, (Fechner et al. 2014, Bosch et al. 2014). Typically a turn rate law is used to represent kite turning in numerical models (Erhard & Strauch 2013).

In this case, pseudo control was implemented in the numerical model similar to that proposed by Williams et al. (2007), and Paiva & Fontes (2018), where the roll angle is controlled to adjust the orientation of the aerodynamic forces acting at the kite point mass. Attitude dynamics were similarly not accounted for. To this end, it was assumed that the kite auto-corrects to align $\vec{X}_k$ with the apparent incoming wind velocity. The yaw turn rate was limited to allow for side slip at low kite velocities, such as is experienced at the edges of the wind window.

2.2.4 *Tether contributions*

It was presumed that due to the short tether length used for the numerical model of less than 500 m, the tether would behave as a straight, rigid rod connecting the kite to the ground station. The mass of the tether was included in the point mass of the kite. At this point the tether drag contribution was assumed to be negligible.

When the tether length is increased the drag effects should be taken into account by adding a quarter of the tether drag area to the kite drag area in the overall drag computation, as shown in Argatov et al. (2011).

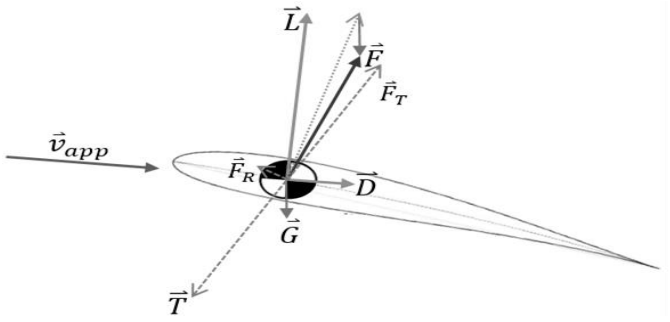

Figure 3: Kite load case

2.3 *Load case*

The load case considered here included both aerodynamic and gravity forces. These forces are depicted in Figure 3. The resultant force was defined by equation

$$\vec{F} = \vec{L} + \vec{D} + \vec{G} \quad (5)$$

Where the corresponding lift ($\vec{L}$), and drag ($\vec{D}$) forces were computed as

$$\vec{L} = \frac{1}{2}\rho A C_L \left|\vec{Y}_k \times \left(\vec{v}_{app} \times \vec{Y}_k\right)\right|^2 \cdot \frac{\vec{Y}_k \times \vec{v}_{app}}{\left|\vec{Y}_k \times \vec{v}_{app}\right|}, \quad (6)$$

and

$$\vec{D} = \frac{1}{2}\rho A C_D \left|\vec{v}_{app}\right|\vec{v}_{app} \quad (7)$$

with air density (ρ) and kite area (A). The axis $\vec{Y}_k$ represents the Y-axis of the kite reference system as illustrated in Figure 1. Finally the gravity force ($\vec{G}$) was computed through

$$\vec{G} = (m_k + m_t)\vec{g} \quad (8)$$

Where m_k, and m_t, indicate the kite and tether mass respectively, and $\vec{g}$ indicates gravitational acceleration.

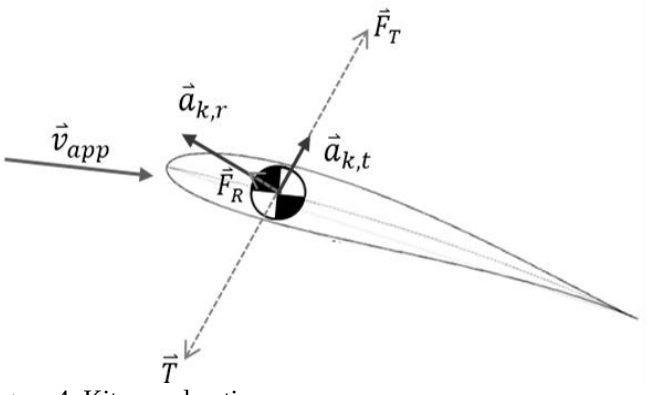

Figure 4: Kite accelerations

The resultant force was divided into two components, tangential ($\vec{F}_T$) and perpendicular ($\vec{F}_R$) to the kite tether, which were determined as follows:

$$\vec{F}_T = \left(\vec{F} \cdot \vec{X}_T\right)\vec{X}_T \quad (9)$$

$$\vec{F}_R = \vec{X}_T \times \left(\vec{F} \times \vec{X}_T\right) \quad (10)$$

Due to the tether length remaining constant, the kite acceleration tangential to the tether ($\vec{a}_{k,t}$) was set to zero such that $\vec{T} = -\vec{L}_T$, as illustrated in Figure 4. Finally, the kite angular kite acceleration ($\vec{a}_{k,r}$) was computed through equation 11.

$$\vec{a}_{k,r} = \frac{\vec{F}_R}{(m_k + m_t)l_T} \quad (11)$$

2.4 *Carousel motion*

For initial analysis, the carousel was modelled to rotate at a set angular velocity. The additional displacement of the kite due to this movement of the tether base was assumed to be in the direction of $\vec{F}_T$, as shown in Figure 5. It was subsequently assumed that the velocity of the tether base would be substantially smaller than that of the kite and thus would have a negligible effect on the kite forces within a single time step iteration. Thus, this displacement solely affected the tether tension ($\vec{T}$) as per the following:

$$\vec{T} = \vec{F}_T - \vec{F}_{T,car}\,, \quad (12)$$

where:

$$\vec{F}_{T,car} = (m_k + m_t)\frac{\vec{d}_k}{dt^2} \quad (13)$$

In equation 13, the kite movement ($\vec{d}_k$) was derived from the carousel movement of the tether base $\vec{d}_b$, the tether vector along $\vec{X}_T$, and the assumption that the tether length remains constant, as illustrated in Figure 5.

The timestep used was set suitably small to prevent significant errors from building up. The carousel effect on the kite displacement was added to the displacement due to the radial acceleration computed through equation 11.

The power take off (P) was subsequently computed using the 'effective' horizontal component of the tether tension in the direction of travel of the base of the tether ($\vec{F}_p$). An efficiency factor (η) was included to account for losses in the system

$$\vec{F}_P = \left(\vec{F}_T \cdot \vec{v}_T\right)\frac{\vec{v}_T}{|\vec{v}_T|^2} \quad (14)$$

$$P = \left|\vec{v}_T \vec{F}_P\right|\eta \quad (15)$$

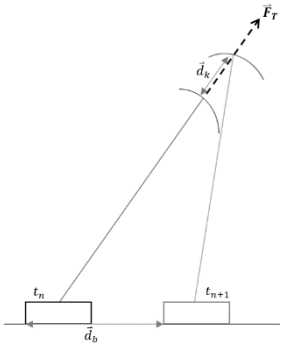

Figure 5: Kite motion due to carousel

3 EXPERIMENTAL MODEL

3.1 *Setup*

The physical kite model included a 10 m^2 Flysurfer Psycho kite, with a 21 m tether connecting to the kite bridle. This kite was fitted out with a Pixhawk unit including GPS and pitot tube. The Pixhawk contains accelerometers, gyrometers, a barometer, an external pitot tube, and GPS transmitter. The measured values get fed through a Kalmann filter and stored. As such the kite position, rotations, and accelerations were recorded. The pitot tube provided the pressure differential at the leading edge of the kite, which was used to derive the kite apparent velocity. The tether base was fixed to a stationary strongpoint through a load cell. The output from the loadcell was amplified and subsequently logged using an M0 Feather Adafruit Adalogger.

The kite was controlled manually through the kite control bar. This input was recorded through a chest mounted GoPro, the position of the control bar was

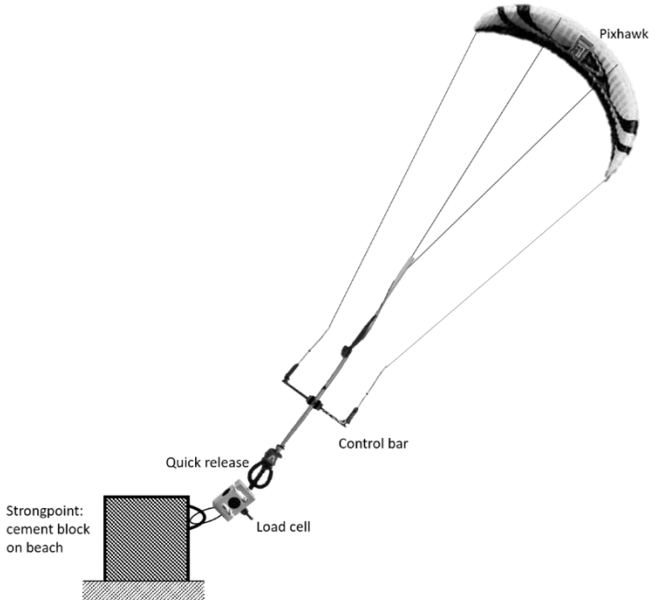

Figure 6: Visual representation of kite setup (not to scale)

Figure 7: Pixhawk and pitot tube mounted in kite bridle

used to deduce what approximate percentage of the maximum control limit input was applied during maneuvres. Turning control is further discussed in section 3.3.

The setup depicted in Figure 6, illustrates the various elements of the physical testing setup, with Figure 7 showing the mounting of the Pixhawk unit with the pitot tube at the leading edge of the kite.

3.2 *Aerodynamic coefficients*

Aerodynamic coefficients of an airfoil such as a kite vary with α as shown earlier in Figure 2. An additional variable often used to relate lift and drag coefficients is the glide ratio: $\gamma = C_L/C_D$. This glide ratio effectively shows the ratio between lift and drag forces across the kite. Due to the assumption of a straight tether, this angle could be deduced from the tether elevation angle (θ_T), found when the kite was at a stationary point down wind, as shown in equation 16 (Alexander & Stevenson 2001).

$$\theta_T = \tan^{-1}\left(\frac{L-G}{D}\right) \tag{16}$$

The aerodynamic coefficients of the kite used, were derived using equations 16, and 6 to 8.

3.3 *Turning control*

Turning control was simulated in the numerical model through imposing a roll angle on the kite represented by a point mass. The roll angle was determined relative to the tether, such that a neutral angle has $\vec{Y}_k$ directly perpendicular to $\vec{X}_T$. This angle was dictated as a percentage of a maximum allowable turn angle.

To determine a realistic scale, the kite was flown in figure 8s. The maximum allowable values were concluded from the measured kite position and attitude combined with the recorded control input throughout the manoeuvre. Subsequently the kite was flown in a successive dive pattern, by initiating maximum impulse turns from zenith.

3.4 *Power control*

The control of tether tension through manipulation of α_0 was modelled from the manual control input through the kite control bar. As in Cadalen *et al.* (2017), this translation from physical control to adjusted α_0 was done as follows:

$$\alpha_0 = K\epsilon + \epsilon_0 \tag{17}$$

Where, ε shows the control input and offset (ε_0), with additional scaling coefficient (K). These coefficients were deduced from the kite response to control variations starting with kite at zenith at the lowest power setting. The control bar was subsequently pulled in to increase α_0. The corresponding location of the kite in the wind window was used to determine the range of α_0 in the Flysurfer kite.

4 RESULTS

In this section the preliminary findings from the initial flight tests are discussed. The results were compared with the findings of the numerical study and deviations between the models are addressed. The resulting carousel model output is also shown and discussed.

4.1 *Aerodynamic coefficients*

Positioning the kite at zenith showed an angle of attach of 10º. This corresponds to a tether elevation angle of 80º, and through equation 16 a glide ratio of 5.7. This lead to the original lift drag coefficients being adjusted to the fit shown in Figure 8. These altered curves fit with the lift and drag coordinates presented by De Lellis Costa de Oliveira (2016).

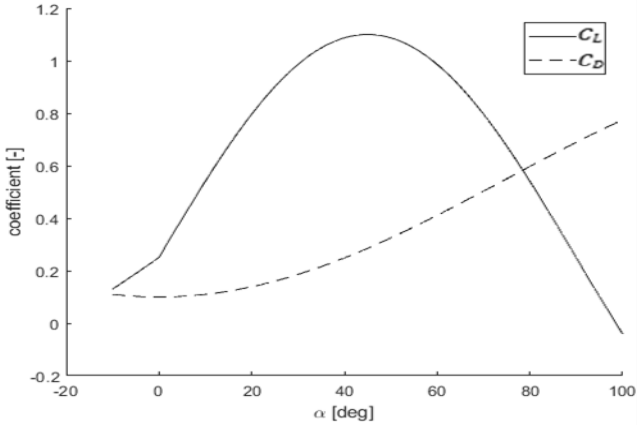

Figure 8: Lift and drag coefficient approximations

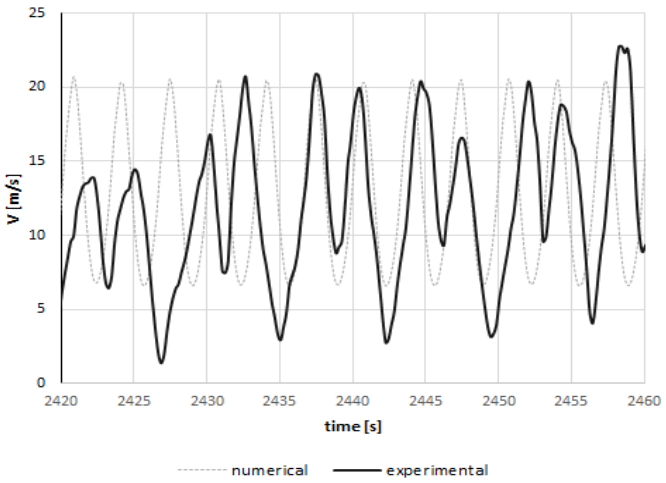

Figure 9: Kite velocity comparison

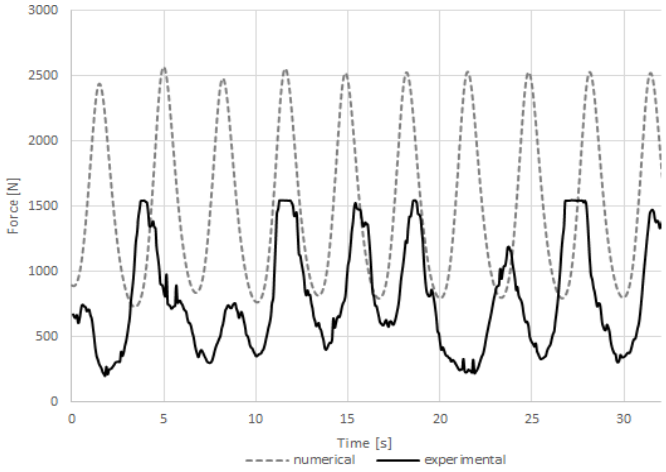

Figure 10: Tether tension comparison

The gyrometer measurements indicated a general yaw rate of up to 3 deg/s when flying in a smooth figure 8 pattern. However, when initiating a steep dive from zenith this rate increased up to 10 deg/s. The yaw limits imposed on the numerical model reflect these limits.

4.2 *Kite velocities*

The kite velocity was both recorded by the GPS unit and can be derived from the data recorded from the accelerometers within the Pixhawk. The resulting kite velocity during a number of figure 8 manoeuvres was compared to the output of the numerical model. This comparison is shown in Figure 9.

While the top velocities reached match up well, it is at the lower end where the results vary more substantially. As the kite approached the end of the wind window it decelerated due to the change in kite orientation, leading to the kite velocity being practically opposite to the wind speed. In the numerical model the turn was initiated before this effect is seen. An automated control system would be able to fine tune the timing of these manoeuvres.

4.3 *Tether tension*

The tension in the main power line was measured throughout the kite test. The results were compared to those gained from the numerical model and are depicted in Figure 10. As with the velocities the numerical model showed a higher predicted load. This was due primarily to the higher velocities computed, as discussed in the previous section. However, a minor portion of the discrepancy was due to the fact that only the load along the main power line was considered, as the load used to steer the kite through the steering lines was not measured during the flight.

Additionally, it was found that the line loading appeared to top out at around 1.5 kN. The kite used during this test is a highly developed design, using the deformability of the wing to produce a consistent pulling force required for kite surfing. As such there are a number ofsafety features to prevent over powering of the kite during such high loading manoeuvres, a feature that is not incorporated in the numerical model.

4.4 *Carousel effects*

Using the adjusted aerodynamic coefficients discussed in section 4.1, the kite carousel model was run to show an initial estimation of generation potential. The results shown in Figure 11 were generated assuming a single airborne kite with a 30 m tether. The carousel modelled had a radius of 3 m and was rotated at 3.5 rpm. A constant wind speed of 6 m/s was assumed. Because only one kite was modelled, the power generated dips into negative values where the kite needed to be dragged upwind.

The power production is highly dependent on the kite flight path. In this case a basic control was used to fly the kite in high power figure 8's while generating, and send it to a low power holding position at zenith during the non-generating part of the carousel

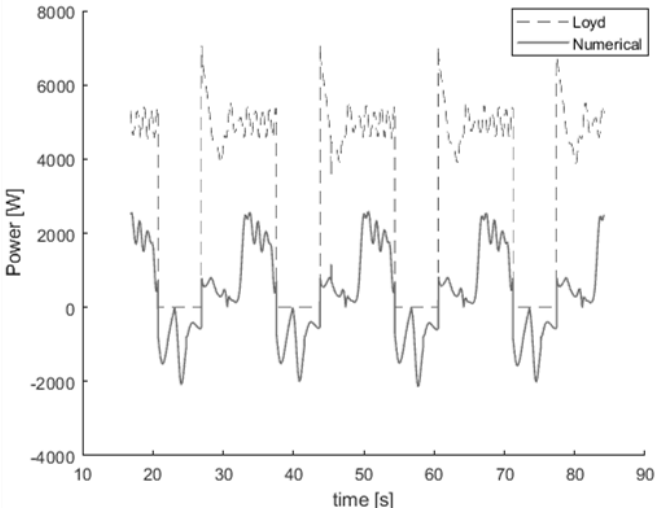

Figure 11: Numerical estimate of power generated by carousel versus Loyd maximum available crosswind power.

cycle. While this rudimentary control strategy caused high power spikes during the transition phase between the powered and non-powered sections of the carousel cycle, it did show a net power production of 360W. Optimizing the carousel design and specifically the kite trajectory leaves room to greatly improve this output.

5 DISCUSSION

The initial numerical results were checked against the theoretical limit of crosswind kite power generation, deduced by (Diehl 2013), from earlier work by Loyd (1980). The equation shown below shows the maximum power potential assuming perfect crosswind flight with an extending tether causing rotation in a ground based generator, at an optimum reel out velocity equal to $\vec{v}_w/3$.

$$P_{Loyd} = \frac{1}{2}\rho V_w^3 A \frac{4}{27}\, C_L \left(\frac{C_L}{C_D}\right)^2 \tag{18}$$

Computing the potential power using the Loyd equation showed a maximum generation of 3 kW, as shown in Figure 11. The Loyd estimate does not take into account the power required to pull the kite upwind, at which point in time the power is set to zero. This check shows that in its current configuration the kite carousel power generation falls substantially beneath the theoretical power limit of crosswind power. Which allows for substantial system improvements due to further optimization of the flightpath and transition between the powered and depowered portions of the generator cycle.

Distinct gains in power can also be made in the transition phases where the kite transitions from low powered glide mode, to high powered generation mode. Figure 11 shows the first half of the generating cycle still sees the kite transferring slowly into a higher powered flightpath. Improving this may require a deviation from the current flightpath of low and high figure 8's to a pattern more tailored to the carousel movement.

With kite power not having reached commercial stages of production, there is limited possibility to compare results with similar kite designs. At the current power estimation this would compare the output of a 3 m wind turbine in 6 m/s winds with an aerodynamic efficiency of 0.4 (Burton et al. 2011).

Further flightpath optimization would lead to a more efficient transition phase, pushing up the net power generation towards the 2kW. This is comparable to the output of a 3.5 m wind turbine under the same conditions.

6 CONCLUSIONS

A minimum order numerical kite model has been introduced, which models a kite generator in a carousel configuration. The kite dynamics have been compared to data gained through experimental testing using a high performance ram air sports power kite.

Subsequently, model parameters including the lift and drag coefficient curves have been adjusted to reflect the practical behaviours of the kite. Although some distinct differences are noted in kite velocity and tether tension between models, this is attributed to the lack of sophisticated kite control in the experimental testing.

Using the updated model to evaluate potential power production of the carousel design showed a net power production of 360W. This can be greatly improved by further optimizing the kite flight path to initiate a more effective transition between when the kite is rotating the generator and when it is being pulled up wind by the generator.

7 FUTURE WORK

Following from this work the carousel model will be subjected to submerged conditions. This includes accounting for added mass and replacing the wind model with a tidal flow.

To deal with this varying flow the control scheme must be adapted to vary flightpath options for optimum generation. Finally the carousel will be expanded to include multiple kites working in unison to provide smooth generation. All of this will lead to a full model that will determine the feasibility of the submerged carousel design.

8 ACKNOWLEDGMENTS

The authors would like to thank the Energy Technology Institute and the Research Council Energy Programme for funding this research as part of the ID-CORE programme (grant EP/J500847), and the Scottish Association for Marine Science for providing technical assistance and equipment.

REFERENCES

Alexander, K, and J Stevenson. 2001. "A Test Rig for Kite Performance Measurement." Proceedings of the Institution of Mechanical Engineers, Part B: Journal of Engineering Manufacture 215 (4): 595–98. https://doi.org/10.1243/0954405011518412.

Argatov, I., P. Rautakorpi, and R. Silvennionen. 2011. "Apparent Wind Load Effects on the Tether of a Kite Power Generator." Journal of Wind Engineering and Industrial Aerodynamics 99 (10): 1079–88. http://dx.doi.org/10.1016/j.jweia.2011.07.010.

Bosch, Allert, Roland Schmehl, Paolo Tiso, and Daniel Rixen. 2014. “Dynamic Nonlinear Aeroelastic Model of a Kite for Power Generation.” Journal of Guidance, Control, and Dynamics 37 (5): 1426–36. https://doi.org/10.2514/1.G000545.

Cadalen, B., P. Lanusse, J. Sabatier, F. Griffon, and Y. Parlier. 2017. “Modeling and Control of a Tethered Kite in Dynamic Flight.” In Innov’Sail 2017. Lorient, France. https://hal.archives-ouvertes.fr/hal-01707611.

Canale, M., L. Fagiano, and M. Milanese. 2009. “KiteGen: A Revolution in Wind Energy Generation.” Energy, WESC 2006Advances in Energy Studies6th World Energy System Conference5th workshop on Advances, Innovation and Visions in Energy and Energy-related Environmental and Socio-Economic Issues, 34 (3): 355–61. https://doi.org/10.1016/j.energy.2008.10.003.

Cherubini, A., A. Papini, R. Vertechy, and M. Fontana. 2015. “Airborne Wind Energy Systems: A Review of the Technologies.” Renewable and Sustainable Energy Reviews 51: 1461–76. http://dx.doi.org/10.1016/j.rser.2015.07.053.

Cherubini, Antonello. 2017. “Advances in Airborne Wind Energy and Wind Drones.” PhD Thesis, Sant’Anna University of Pisa. https://www. areasciencepark. it/wp-content/uploads/PHD_THESIS-Cherubini. pdf.

Dadd, G. M., D. A. Hudson, and R. A. Shenoi. 2010. “Comparison of Two Kite Force Models with Experiment.” Journal of Aircraft 47 (1): 212–24. https://doi.org/10.2514/1.44738.

De Lellis Costa de Oliveira, Marcelo. 2016. “Airborne Wind Energy with Tethered Wings: Modeling, Analysis and Control.” PhD Thesis. https://doi.org/10.13140/RG.2.2.12207.74409.

Diehl, Moritz. 2013. “Airborne Wind Energy: Basic Concepts and Physical Foundations.” In Airborne Wind Energy, edited by Uwe Ahrens, Moritz Diehl, and Roland Schmehl, 3–22. Berlin, Heidelberg: Springer Berlin Heidelberg. https://doi.org/10.1007/978-3-642-39965-7_1.

Erhard, Michael, and Hans Strauch. 2013. “Theory and Experimental Validation of a Simple Comprehensible Model of Tethered Kite Dynamics Used for Controller Design.” In Airborne Wind Energy, 141–65. Green Energy and Technology. Springer, Berlin, Heidelberg. https://doi.org/10.1007/978-3-642-39965-7_8.

Fagiano, L. 2009. “Control of Tethered Airfoils for High-Altitude Wind Energy Generation.” PhD Thesis, Politecnico di Torino.

Fechner, U. 2016. “A Methodology for the Design of Kite-Power Control Systems.” https://doi.org/10.4233/uuid:85efaf4c-9dce-4111-bc91-7171b9da4b77.

Fechner, Uwe, Rolf van der Vlugt, Edwin Schreuder, and Roland Schmehl. 2014. “Dynamic Model of a Pumping Kite Power System.” *ArXiv:1406.6218 [Cs]*, June. http://arxiv.org/abs/1406.6218.

Geschiere, Nick H. 2014. “Dynamic Modelling of a Flexible Kite for Power Generation.” MSc Thesis, TU Delft. http://www.lr.tudelft.nl/fileadmin/Faculteit/LR/Organisatie/Afdelingen_en_Leerstoelen/Afdeling_AEWE/Wind_Energy/Education/Masters_Projects/Finished_Master_projects/doc/Nick_Geschiere_r.PDF.

Ippolito, Massimo. 2009. “KiteGen Research » KiteGen Carousel.” April 9, 2009. http://www.kitegen.com/en/products/kite-gen-carousel/.

Khan, Zeashan, and Muhammad Rehan. 2016. “Harnessing Airborne Wind Energy: Prospects and Challenges.” *Journal of Control, Automation and Electrical Systems* 27 (6): 728–40. https://doi.org/10.1007/s40313-016-0258-y.

Losantos, L. Salord, and G. Sánchez-Arriaga. 2015. “Flight Dynamics and Stability of Kites in Steady and Unsteady Wind Conditions.” *Journal of Aircraft* 52 (2): 660–66. https://doi.org/10.2514/1.C032825.

Loyd, M. L. 1980. “Crosswind Kite Power.” *Journal of Energy* 4 (3): 106–11. https://doi.org/10.2514/3.48021.

Paiva, Luís, and Fernando A. C. C. Fontes. 2018. “Optimal Control Algorithms with Adaptive Time-Mesh Refinement for Kite Power Systems.” *Energies* 11 (February): 475. https://doi.org/10.3390/en11030475.

Pastor-Rodríguez, A., G. Sánchez-Arriaga, and M. Sanjurjo-Rivo. 2017. “Modeling and Stability Analysis of Tethered Kites at High Altitudes.” *Journal of Guidance, Control, and Dynamics* 40 (8): 1892–1901. https://doi.org/10.2514/1.G002550.

Spera, D. A. 2008. “Models of Lift and Drag Coefficients of Stalled and Unstalled Airfoils in Wind Turbines and Wind Tunnels.” NASA nasa/cr-2008-215434. https://ntrs.nasa.gov/archive/nasa/casi.ntrs.nasa.gov/20090001311.pdf.

Stull, Roland B. 2000. Meteorology for Scientists and Engineers. Brooks/Cole.

Vlugt, R. van der, A. Bley, M. Noom, and R. Schmehl. 2017. “Quasi-Steady Model of a Pumping Kite Power System.” ArXiv:1705.04133 [Cs, Math], May. http://arxiv.org/abs/1705.04133.

Williams, P., B. Lansdorp, and W. Ockels. 2007. “Optimal Trajectories for Tethered Kite Mounted on Vertical Axis Generator.” In AIAA Modeling and Simulation Technologies Conference and Exhibit. Hilton Head, South Carolina. http://dx.doi.org/10.2514/6.2007-6706.